Available online at www.sciencedirect.com
SCIENCE DIRECT®
Organic Geochemistry 35 (2004) 379–392
Organic Geochemistry
www.elsevier.com/locate/orggeochem

Methane generation from coal during open system pyrolysis investigated by isotope specific, Gaussian distributed reaction kinetics

Bernhard Cramer*

Federal Institute for Geosciences and Natural Resources (BGR), Stilleweg 2, 30655 Hannover, Germany

Abstract

A reaction kinetic model is presented to differentiate individual complexes of reactions of the thermal decomposition of sedimentary organic matter during pyrolysis experiments. This model is applied to methane generation from coal during open system pyrolysis experiments with linear heating. The reaction kinetic model is based on the concept of a certain number of reaction complexes contributing to the generation of the product methane, each reaction complex distinguished by an initial pool of precursor sites with a defined stable carbon isotope signature and a common reaction rate determining step. For each reaction the mathematical model defines Gaussian distributed activation energies, a single pre-exponential factor, an initial isotope ratio of the precursor and a single difference in activation energy between the heavy and the light isotope species. Based on this concept, stable carbon isotopes and the dynamics of thermal methane generation from a Carboniferous coal with 0.72% vitrinite reflectance are explained with a set of four independent reactions. It is suggested that these reactions represent the following pathways (listed in the order of occurrence): (I) reactions involving the cleavage of thermally unstable C–O and C–S bonds, (II) demethylation, (III) release of groups which cross link ring structures and/or secondary cracking of long chain hydrocarbons within the molecular network of the coal, and (IV) polymerisation and condensation reactions. Reactions II and III contribute the major part to total methane potential. However, the addition of the minor reactions I and IV has significant influence on the stable carbon isotope trend of methane.

1. Introduction

The stable isotope distribution of carbon and hydrogen in methane and its homologues are the most important chemical characteristics of natural gas. They can be used to decipher the processes of gas generation, for example thermal or microbial gas generation (Schoell, 1980), to distinguish between microbial gas from CO_2-reduction and that from fermentation (Whiticar et al., 1986), to deduce the type and maturity of thermally generated gas (Stahl and Carey, 1975; Faber, 1987; Berner and Faber, 1996), and to investigate migrational processes during the passage of the gas from its origin through the rocks of the Earth's crust (Prinzhofer and Pernaton, 1997). These widely applied classification schemes are based mostly on empirical relationships where certain ranges of isotopic patterns or isotope effects were attributed to specific gas generating processes or specific source rocks and maturities. Whilst it is obvious that isotopic distribution of natural gas components is governed by processes during gas generation, none of the empirical classification schemes relates the isotopic pattern directly to the progress of hydrocarbon generation.

First attempts to link the isotopic composition of individual gas components to the process of hydrocarbon generation were focused on Rayleigh distillation equations (Berner et al., 1995; Clayton, 1991; Galimov,

* Corresponding author.
E-mail address: b.cramer@bgr.de (B. Cramer).

0146-6380/$ - see front matter © 2004 Elsevier Ltd. All rights reserved.
doi:10.1016/j.orggeochem.2004.01.004

1988; Rooney et al., 1995). Because Rayleigh distillation equations do not consider the temperature dependence of isotope fractionation, the applicability of most of these models is limited (Lorant et al., 1998). According to Bigeleisen (1949) the effect of isotope partitioning during chemical reactions usually is caused by differences between the reaction velocities of the individual isotope species. In consequence, isotope specific reaction kinetic parameters were used to describe gas generation and associated isotope fractionation during pyrolysis experiments (Gaveau et al., 1987; Cramer et al., 1998).

Rooney et al. (1995) pointed out that a major limitation in developing isotopic models for natural gas is uncertainty about the mechanisms of gas generation. Recent work has used theoretical calculations of model parameters to predict gas generation from sedimentary organic matter (Payne and Ortoleva, 2001) and stable carbon isotopes of methane in natural gas (Tang et al., 2000).

Another approach uses the generation dynamics of individual gas components during pyrolysis experiments to differentiate individual reaction mechanisms. From these measurements it was evident that the generation of gas components from coaly organic matter could not easily be explained with single first order reactions. Methane generation from coal during pyrolysis experiments was either related to three individual reactions (Kröger and Brücker, 1961; Jüntgen and van Heek, 1970; Campbell, 1978; van Heek at al., 1986) or to four reactions (Jüntgen, 1964; Hanbaba et al., 1968).

Measured stable carbon isotope trends of the generated methane during pyrolysis experiments gave additional evidence for the contribution of distinct reactions to bulk generation (Fig. 1). From the data shown in Fig. 1 Friedrich and Jüntgen (1973) suggested that two reactions are responsible for methane generation from coal. Inflexions in the $\delta^{13}C$ trend and inverse isotope trends of methane (Fig. 1) were thought to be due to these reactions being overwhelmed by individual, subsequent reactions. Other investigations based on the isotope composition of methane proposed three reactions (Rohrback et al., 1984; Gaveau et al., 1987).

In this context, the main objective of this paper is to investigate the reactions of methane generation during thermal decomposition of coal based on high resolution stable carbon isotope data on methane generated during dry, open system pyrolysis. These data are taken from a previous publication which was focussed on the applicability of reaction kinetic isotope modelling to geological systems (Cramer et al. 2001). After an introduction into the mathematics of first order reaction kinetics, isotope dynamics of single reactions as well as of distributed reaction complexes are derived theoretically. Finally, after application of a multi-reaction approach, reaction mechanisms of methane generation during the pyrolysis experiments will be suggested.

2. Reaction kinetic concept of gas generation and stable isotope fractionation

2.1. Single first-order reactions

The mathematics of reaction kinetics recently have been reviewed comprehensively by Schenk et al. (1997)

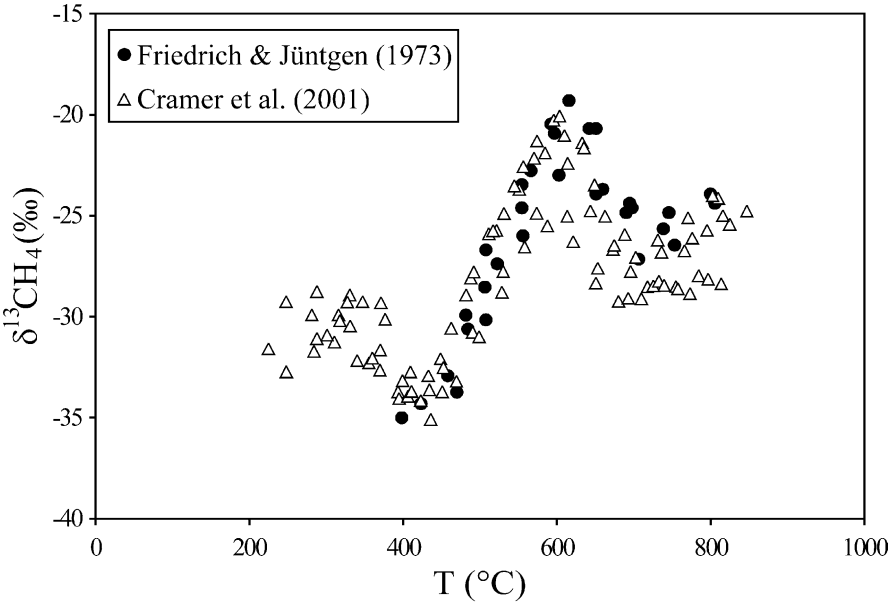

Fig. 1. Published trends of stable carbon isotope ratios of methane thermally generated from coal during dry, open system pyrolysis with 2 K/min heating.

and Burnham and Braun (1999). The basis of the reaction kinetic concept usually applied is the temperature dependence of the rate coefficient $k(T)$, which is assumed to have the Arrhenius form, including a pre-exponential factor A (s^{-1}) (frequently termed frequency factor or Arrhenius factor), the activation energy E (J/mol) and the gas constant G (8.3145 J/K/mol):

$$k(T) = A \cdot \exp\left(-\frac{E}{G \cdot T}\right) \quad (1)$$

Applying this, the rate of product generation r, the amount of reaction product c and the amount of residual reactant f can be calculated as functions of temperature T and time t. A brief summary of the underlying mathematics is given in Appendix A1.

A heavy isotope species of a given molecule in a given chemical bond usually has a slightly lower zero-point energy and higher activation energy than the corresponding light isotope species. This difference in bond energy will affect the kinetics of the thermal cleavage of the bond. Considering that this cleavage is the rate determining step of the reaction, the two isotope species of the product will be generated at different rates. This leads to an isotope separation between the reactant and the product. The factor by which isotopes are separated during kinetic chemical reactions usually is termed the kinetic isotope effect *KIE*. According to Bigeleisen (1949) the *KIE* can be defined as the ratio of the rate constants of the formation of the two isotopic molecules. With the Arrhenius-type temperature dependence of the reaction rates of the first-order reaction given in Eq. (1), the kinetic isotope effect is defined by the ratio of the pre-exponential factors R_A as well as the difference in activation energy ΔE between the heavy isotope species H and the light isotope species L:

$$KIE(T) = \frac{k_L(T)}{k_H(T)} = \frac{A_L}{A_H} \cdot \exp\left(\frac{E_H - E_L}{G \cdot T}\right) = R_A \cdot \exp\left(\frac{\Delta E}{G \cdot T}\right) \quad (2)$$

The temperature dependence of the *KIE* in Eq. (2) must be considered as an ideal approximation because much more complex temperature dependencies with minimum and maximum values and *KIE*-values below 1 (so called crossovers) have been described (Stern et al., 1968; Spindel et al., 1970). Nevertheless, Eq. (2) represents the most common form of $KIE(T)$ and was appropriate to model isotope fractionation associated with light hydrocarbon generation from coal during pyrolysis experiments (Cramer et al., 1998).

For isotope calculations a certain isotope ratio R (Appendix A2) of the initial precursor at the beginning of the reaction R_{prec0} is assumed. During the process of reaction the product is generated and the precursor is subsequently exhausted. Due to the slight differences in the reaction rates of the isotope species, isotope ratios of the residual reactant R_{prec}, of the instantaneous product R_{inst}, as well as of the cumulative product R_{cum} will change. By defining specific amounts of the initial and the residual reactant (f_{H0} and f_{L0}, f_H and f_L) as well as specific amounts of the reaction product (c_H and c_L) these isotope ratios can be defined for single first-order reactions as functions of time and temperature (Appendix A2).

These definitions provide the basis for calculating the isotope ratios of the precursor, of the instantaneous product as well as of the cumulative product at any stage of the reaction (Fig. 2). As indicated in Fig. 2, at the beginning of the reaction the precursor isotope signature does not change significantly. Although isotope fractionation at low temperatures is much more significant, the pool of precursor groups is not sufficiently altered due to product generation to result in significant changes in $\delta^{13}C_{prec}(T)$. Accordingly, product isotope ratios do not change rapidly either. Nevertheless, starting from the lowest temperature the product is enriched in the light isotope species in comparison to the precursor. During this early phase of the reaction the difference in isotope ratios between the precursor and the product slightly decreases with increasing temperature (Fig. 2) mirroring mainly the temperature dependence of the *KIE* [Eq. (2)].

At the temperature of maximum generation of the light isotope species (T_{max}) the instantaneous isotope ratio of the product passes the initial isotope ratio of the precursor. At the end of the main phase of product generation the isotope ratio of the cumulative product approaches the initial isotope ratio of the precursor, indicating that the majority of the precursor groups have undergone reaction. With further reaction the *KIE* causes a strong enrichment in the heavy isotope species finally resulting in infinitely high $\delta^{13}C$ values of precursor and instantaneous product (Fig. 2).

2.2. Distributed first-order reactions

Kerogen is a complex material and in most cases its thermal decomposition cannot be described adequately with a single reaction model (Hanbaba et al., 1968). To handle this situation it is assumed that the complexity of such a reaction can be expressed by a number of independent, parallel first-order reactions. In principle, each of these reactions is characterized by distinct values of activation energy and pre-exponential factor. In practise, it can be assumed that the pre-exponential factor is identical for the whole set of reactions, therefore the rate coefficients differ only in activation energy. The fact that such models with constant pre-exponential factors have been applied successfully in many cases, indicates that

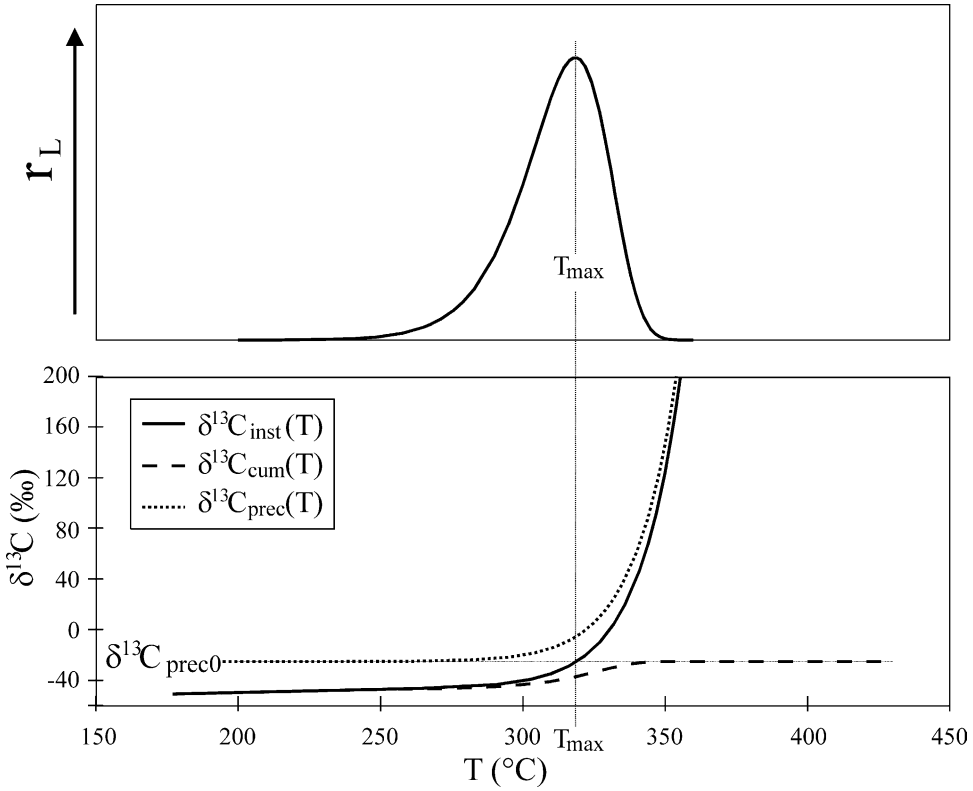

Fig. 2. Generation rate r_L of the dominating ^{12}-species and δ^{13}C-values of the product and the precursor as function of temperature of a first-order reaction with $E_L = 200$ kJ/mol, $A = 10^{15}$ s^{-1}, and $f_{L0} = 1$, constantly heated at 2 K/min. The initial δ^{13}C-value of the precursor is −25 ‰. Isotope fractionation is caused by a difference in activation energy of 100 J/mol with equal pre-exponential factors.

the entropies of formation of activated complexes leading to the release of particular species are in fact quite similar (Suuberg, 1983).

One approach to describe an activation energy distribution of a reaction divides the energy spectrum into a certain number of discrete activation energies with individual reaction probabilities, or in other words, with individual initial generation potentials (Tissot, 1969). Another approach treats the reaction with an infinite number of parallel first-order reactions (Hanbaba et al., 1968). The activation energies of these reactions are then represented by a continuous probability function $D(E)$ (“density function”). This model of a distributed reaction is still a simplification because real probability functions are not known in general. In petroleum generation studies different types of distribution functions have been applied successfully (Burnham and Braun, 1999), but for practical use Gaussian distributions are used most frequently (Anthony and Howard, 1976, Braun and Burnham, 1987; Burnham et al., 1987; Hanbaba et al., 1968; Jüntgen and van Heek, 1970; Lakshmanan et al., 1991; Sundararaman et al., 1992; Suuberg, 1983). Compared to other continuous probability functions applied to thermal decomposition experiments, the Gaussian distribution is the simplest. With the Gaussian distribution parameter σ (standard deviation) only one additional variable number is involved compared to the single reaction model (Appendix B1). Because of their symmetry, Gaussian activation energy distributions in many cases were not appropriate to account for asymmetric generation dynamics. These asymmetric generation trends were then modelled applying Weibull energy distributions or pseudo n-th order models (Burnham and Braun, 1999). For the mathematical modelling of methane generation from coal presented here, observed asymmetric generation trends are simulated by introducing a set of independent Gaussian reaction complexes contributing to the product methane.

For the development of a model of isotope specific reaction continuums, additional prerequisites have to be defined. In accordance with the simplification that the pre-exponential factor is identical over the entire reaction spectrum, it is furthermore assumed that the ratio of the isotope specific pre-exponential factors R_A is also constant. In addition, the ratio of the reaction probabilities of the heavy to the light isotope species is set to be distributed uniformly. So, an equal initial isotope ratio of the pseudo-precursors at each point of the

probability function $D(E)$ is defined which is identical to the overall initial isotope ratio of the precursor R_{prec0}. Isotope fractionation is then caused by differences in the activation energy spectrum between the density functions of both isotope species which is defined to be constant over the entire probability function. Considering these prerequisites, for distributed first-order reactions the isotope ratios of the precursor $R_{prec}(T)$, of the cumulative product $R_{cum}(T)$, and of the instantaneous product $R_{inst}(T)$ can be expressed according to Appendix B2.

For a Gaussian distributed reaction the influence of the distribution parameter σ on the generation rate and on the isotope ratio of the instantaneous product is shown in Fig. 3. Starting with the reaction given in Fig. 2 the σ-value is increased up to 12% of E_0. This increase of σ causes obvious changes in the isotope trend of the instantaneous product $\delta^{13}C_{inst}(T)$. At higher temperatures, the model of Gaussian distributed reactions results in an almost linear increase of the isotope ratios with increasing temperature (Fig. 3). At σ values above about 5% the instantaneous isotope trends show a pseudo-linear increase with temperature over the entire displayed range of conversion. In common with single first-order reactions, the isotope trends of the instantaneously generated product for all distributed reactions pass the initial isotope ratio of the precursor at the temperature of the maximum generation rate T_{max} (Fig. 3).

All reactions in Fig. 3 were calculated applying an identical $KIE(T)$ with $R_A = 1$ and $\Delta E = 100$ J/mol according to Eq. (2). Nevertheless, the slopes of the pseudo-linear trends decrease with increasing σ. A wide distribution of activation energies seems to suppress isotope fractionation. This effect was first described by Galimov (1974) who stated that the degree of isotope fractionation in a distributed reaction is significantly lower than in a single reaction. In fact, isotope fractionation as defined with a kinetic isotope effect [Eq. (2)] is not lower. For distributed reactions at each temperature a wide range of activation energies contributes to the bulk process, each of them with the same $KIE(T)$. The bulk isotope trends (Fig. 3) represent a smoothed mixture of this wide spectrum of individual reaction sites. With increasing width of the activation energy distribution a wider energy spectrum contributes to the

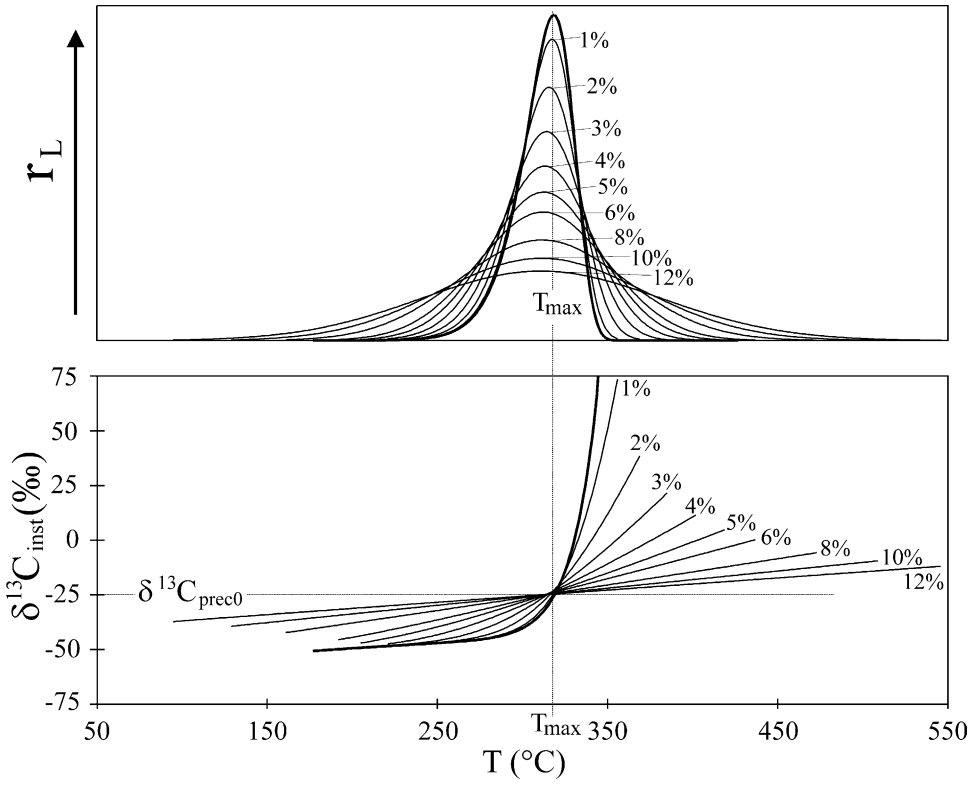

Fig. 3. Generation of the light carbon isotope species r_L and stable carbon isotope ratios of the instantaneous product ($\delta^{13}C_{inst}$) generated from Gaussian distributed reactions heated at 2 K/min. The bold solid line indicates the trend for the reaction shown in Fig. 2 based on reaction kinetic parameters defined there. The thin solid lines display the influence of increasing σ-values of a Gaussian distributed reaction complex on these trends. The corresponding values of σ are given in% of the mean activation energy E_0 (200 kJ/mol).

bulk reaction. In consequence, the spectrum of isotope values contributing to the bulk isotope trend increases and the bulk trend becomes flatter. So, an increasing σ-value may have the same effect on the trend of $\delta^{13}C_{inst}$ as a decreasing $KIE(T)$ and vice versa.

Examples of this "isotope compensation effect" are shown in Fig. 4. The reactions displayed differ only in ΔE and σ. Three pairs of isotope trends are shown where one reaction with a comparatively high σ-value and a high ΔE has a very similar $\delta^{13}C_{inst}$-trend as a reaction with low σ-value and low ΔE.

2.3. Combined reaction systems

To describe thermal methane generation from coal and the associated stable carbon isotope distribution, a reaction system of i independent Gaussian distributed reaction complexes is assumed. These individual reactions reflect independent reactant pools, each of them contributing to the product generated. In accordance with the models of single and distributed reactions presented above, each reactant pool is characterised by an individual isotopic inventory and individual reaction kinetic parameters. The generation of the overall product as well as its isotope composition can be calculated by summing up the contributions of i individual reactions (Appendix C).

In Fig. 5, the differential generation curve and the instantaneous isotope trend are displayed for a reaction system consisting of two independent Gaussian distributed reactions. The two reactions differ in all reaction kinetic parameters, except for the initial isotope ratio of the precursors ($\delta^{13}C_{prec0} = -25$ ‰) (Fig. 5). The minor first reaction I ($f_0 = 6\%$) precedes a widely distributed dominating reaction II ($f_0 = 94\%$). In the differential bulk generation curve the minor reaction can be distinguished only as a weak shoulder.

In contrast, the instantaneous isotope trend is significantly altered by the admixture of the minor reaction. At lower temperature the minor reaction (I) contributes enough isotopically distinct product to cause a significant shift in the bulk isotope trend (Fig. 5). During main product generation the bulk isotope trend is identical to the trend of the dominating reaction because reaction I does not generate sufficient amounts of the product to have significant influence. The reaction system in Fig. 5 is only one possibility of mixing individual reaction complexes. However, from the example in Fig. 5 it is obvious how valuable detailed information on the stable isotope distribution can be to elucidate reaction mechanisms.

3. Modelling of methane generated from coal

Methane generation and associated stable carbon isotope fractionation from coal was investigated in an open system pyrolysis unit, designed for dry, non-isothermal experiments at variable heating rates, online coupled to an isotope ratio mass spectrometer. This method provides high resolution insight into the dynamics of the generation and isotope fractionation of individual gas components from sedimentary organic matter. As gaseous products are permanently flushed

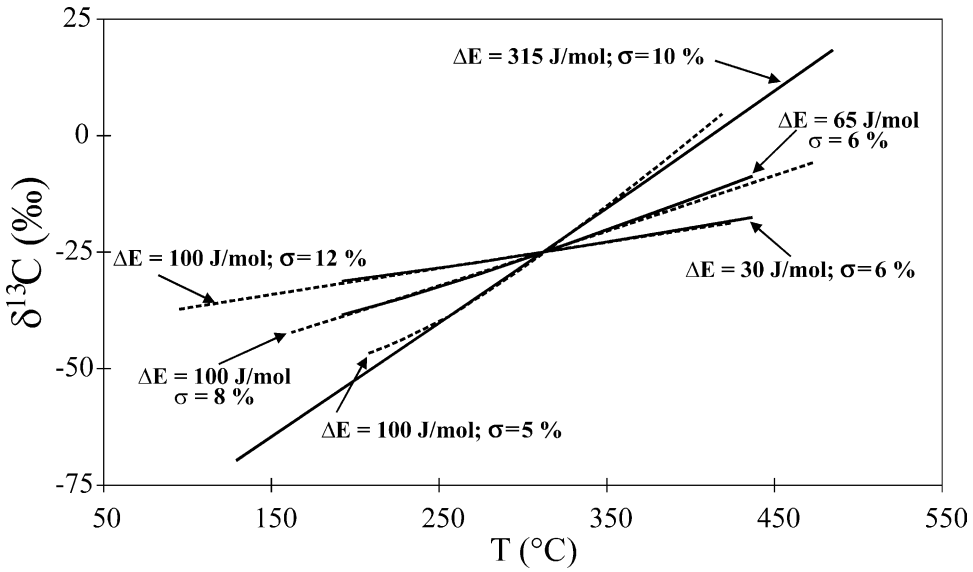

Fig. 4. Three examples to show how the width of a distributed reaction compensates for the kinetic isotope effect. The distributed reaction complexes differ only in ΔE and σ-values. The basic reaction is the same as displayed in Fig. 2. The parameters of the three pairs of isotope trends are shown in the plot.

out of the heated reactor with an inert carrier gas, primary cracking reactions are believed to be the dominating process of gas generation. Detailed descriptions of the pyrolysis method applied as well as the analytical procedures of gas separation and quantification are given in Cramer et al. (2001).

For reaction kinetic modelling only methane, as the most important component of natural gas, is taken into account. Cramer et al. (2001) investigated gas generation from three different coals. Isotope patterns of methane displayed very similar trends for the three coals. So, only the methane data of coal A (Cramer et al., 2001) are used as an example. Coal A is a humic coal from Germany of Upper Carboniferous age, characterized by a vitrinite reflectance of 0.72 R_o and a $\delta^{13}C$ value of bulk organic carbon of −24.6 ‰. Detailed geochemical information as well as the original gas and isotope data from the pyrolysis experiments are provided in Cramer et al. (2001).

Fig. 6 displays the generation dynamics and the isotope trend of methane from coal A during a pyrolysis experiment with 0.2 K/min heating. Measured stable carbon isotope ratios of methane during pyrolysis experiments of coal A show one minimum value at the beginning of bulk generation (350 °C), one maximum (560 °C) and a second minimum value (660 °C) at the end of the reaction (Fig. 6). According to the reaction systems presented in Fig. 5, methane from coal A might be interpreted as the result of the mixing of three individual reaction complexes. From the measured isotope trend there is a single indication that three reactions are not sufficient to explain the data. Around the temperature of maximum methane generation (440 °C) a weak inflexion in the trend of $\delta^{13}C_{inst}$ occurs resulting in a slightly convex line (Fig. 6). Using a multi-reaction-model (Fig. 5) neither one single reaction nor a distributed reaction system as defined above can produce such a convex isotope trend. Consequently, it is inferred

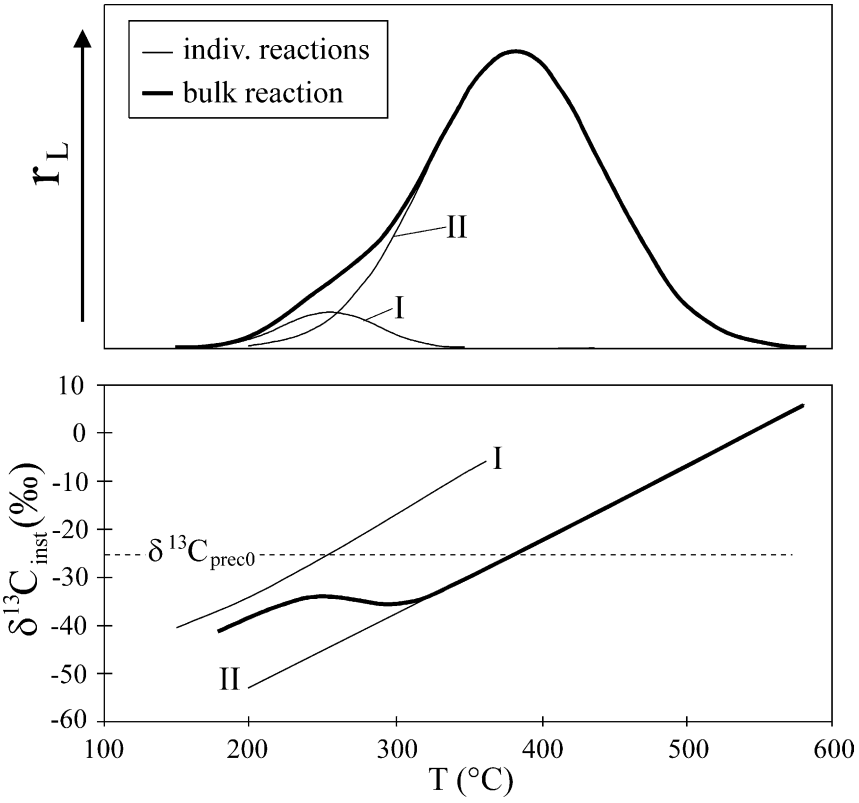

Fig. 5. Generation of the light carbon isotope species r_L and stable carbon isotope ratios of the instantaneous product ($\delta^{13}C_{inst}$) for a reaction system consisting of two independent Gaussian distributed reaction complexes (thin solid lines I and II) contributing to one common product (bold solid line, "bulk reaction"). The heating rate is 2 K/min. The reaction kinetic characteristics of the two individual distributed reactions are:

I—$f_0 = 6\%$, $E_0 = 175$ kJ/mol, $A_L = 10^{14.5}$ s^{-1}, $\delta^{13}C_{prec0} = -25$ ‰, $R_A = 1$, $\Delta E = 65$ J/mol, $\sigma = 5\%$.
II — $f_0 = 94\%$, $E_0 = 225$ kJ/mol, $A_L = 10^{15}$ s^{-1}, $\delta^{13}C_{prec0} = -25$ ‰, $R_A = 1$, $\Delta E = 200$ J/mol, $\sigma = 10\%$.

that this convex occurrence is the result of mixing two parallel reaction complexes. The total isotope trend of methane reflects a system of four independent reaction complexes. As mentioned above, this model of four independent methane generating reactions is in accordance with other published investigations on gas generation from coal during laboratory pyrolysis experiments which did not consider stable carbon isotope evolution (Hanbaba et al., 1968; Jüntgen, 1964).

In order to reduce the number of unknown parameters in the model, the pre-exponential factors of the four reactions were assumed to be identical. A common pre-exponential factor of $2.4 \cdot 10^{14}$ s^{-1} was calculated by applying the method introduced by van Heek and Jüntgen (1968) where the change in the temperature of maximum product generation T_{max} with heating rate is used. The data for this procedure were taken from additional pyrolysis experiments with 0.7 and 2.0 K/min heating rates (Cramer et al., 2001). The reaction specific mean activation energies E_{0i}, the generation potentials f_{0i}, and the distribution parameters σ_i of the four reactions were then calculated by fitting the mixed bulk generation curve to the measured methane generation. With this procedure, the width of activation energy distribution was defined from the dynamics of methane generation. Therefore, one of the parameters influencing apparent isotope fractionation (Fig. 4) was revealed independently from measured isotope dynamics.

The difference in activation energy together with the initial stable carbon isotope ratio of the precursor was calculated by matching the modelled bulk isotope trend of all reactions to the measured values. As an additional simplification, pre-exponential factors of both isotope species were set to be identical ($R_{Ai}=1$). Thus, the difference in activation energy ΔE_i remains as the only parameter in the model defining the $KIE_i(T)$ [Eq. (2)]. Tang et al. (2000) calculated R_A values mostly in the range between 1.02 and 1.04. The underestimation of isotope fractionation with a R_A value of 1 in the model presented here is mainly compensated by higher ΔE values. The modelled and measured generation and isotope curves and the characteristics of the four individual reaction complexes are shown in Fig. 6. The accompanying reaction kinetic parameters are listed in Table 1.

The four reaction complexes almost perfectly match the measured generation and isotopic pattern of methane from coal A (Fig. 6). With an identical pre-exponential factor the mean activation energies lie between

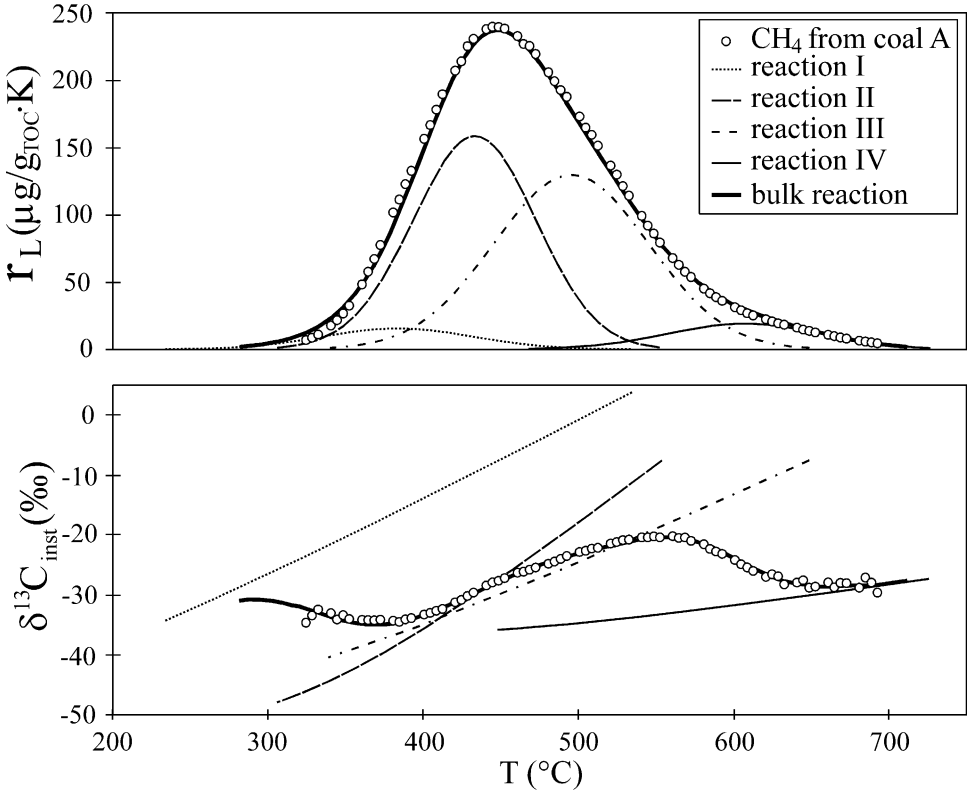

Fig. 6. Generation of $^{12}CH_4$ (r_L) and $\delta^{13}C_{inst}$ of methane from coal A measured during dry, open-system pyrolysis with 0.2 K/min heating. Measured data are taken from Cramer et al. (2001). Reaction kinetic characteristics of the four model reactions are listed in Table 1.

Table 1
Reaction kinetic characteristics of the Gaussian distributed first-order reactions describing methane generation and stable carbon isotope distribution of methane pyrolytically derived from coal (Fig. 6). The coal pyrolysed is of Upper Westphalian age from Germany (Cramer et al., 2001).

	Reaction I	Reaction II	Reaction III	Reaction IV
E_{0i} (kJ/mol)	230	247.5	270	310
A ($^1/_s$)	$2.4 \cdot 10^{14}$	$2.4 \cdot 10^{14}$	$2.4 \cdot 10^{14}$	$2.4 \cdot 10^{14}$
f_{0i} (%)	5.3	43.4	44.7	6.6
σ_i (%)	7	5	6	7
$\delta^{13}C_{prec0i}$ (‰)	−16	−30	−25	−31.5
δE_i (J/mol)	110	100	100	30

230 and 310 kJ/mol (Table 1). Interestingly, the reactions with lowest and highest mean activation energy (I and IV) have the most pronounced effect on the trend of $\delta^{13}C_{inst}$ whereas together they contribute only about 12% to the total methane generation potential (Table 1). The two dominating reactions (II and III) with mean activation energies of 247.5 and 270 kJ/mol have the same initial generation potential of about 44%. Together they cause the continuous increase in $\delta^{13}C_{inst}$ during main methane generation (Fig. 6).

The observation that reaction III results in a smoothed continuation of the isotope trend of reaction II must be realised in the model by a significant difference in $\delta^{13}C_{prec0i}$ of 5 ‰ (Table 1). Whereas isotopic fractionation is identical for both reactions ($\Delta Ea = 100$ J/mol), this shift of 5 ‰ towards an isotopically heavier precursor of reaction III compensates for the isotopic off-set caused by the temperature effect of the higher mean activation energy of reaction III. As a consequence, the isotopic transition between reactions II and III does not occur as a step in the isotope trend but as smoothed convex transition to a flatter slope in the $\delta^{13}C_{inst}$ trend.

4. Proposed reaction pathways

Reaction complex I: It is suggested that reaction complex I generates methane by breaking bonds between carbon and hetero atoms, especially sulphur and oxygen. These bonds are known to be weaker than C–C bonds and release methyl groups at lower temperature (van Krevelen et al., 1951; Smith et al., 1985; Tang et al., 2000). The demethylation of methoxyl groups is often considered one of the most important first steps of early coalification (Gaveau, et al. 1987, del Rio et al., 1994).

With an O/C ratio of 0.15 and S/C ratio of 0.012 (Cramer et al., 2001) large portions of its oxygen and sulphur have already been removed from coal A during diagenesis and early coalification. So the occurrence of reaction I (Fig. 6) can be interpreted as a final stage of the chemical process. Consequently, the set of modelling parameters for reaction I (Table 1) does not reflect the real reaction kinetic parameters of the reaction. It is probable that the calculated mean activation energy of 230 kJ/mol has undergone a shift to higher values due to natural pre-maturation. This effect may also be responsible for the slight overestimation of methane generation with reaction I at temperatures below 350 °C. Probably, a truncated activation energy distribution would have been more appropriate to describe reaction complex I. Another indication for the effect of pre-maturation is the modelled heavy isotope signature of the methane precursor of reaction I with a $\delta^{13}C$ of −16 ‰ (Table 1). Methane generation during burial preferentially removed the light isotope species of reaction I from the system leaving the remaining precursor relatively enriched in the heavy isotope.

Reaction complex II: Reactions II and III are characterized by about the same generation potential, together contributing the main part of methane generation with about 88% of the total potential (Table 1). The isotopic contribution of these reactions to the overall $\delta^{13}C$ trend of methane is responsible for the steady increase of the $\delta^{13}C$ during main methane generation (Fig. 6). This is in accordance with published data on maturity trends of the $\delta^{13}C$ of methane in natural gas from humic organic matter (e.g. Stahl and Carey, 1975; Faber, 1987).

The overall occurrence of both reactions in the reaction kinetic model (Table 1) is similar with a small difference in σ of 1% and identical ΔEa values of 100 J/mol. Differences between the modelled reaction complexes (II and III) are the lower mean activation energy of reaction II and the initial isotope signatures of its precursors (Table 1).

For the pyrolysis experiment, the temperature range of methane generation due to reaction II is between 300 and 500 °C (Fig. 6) which coincides with the temperature range of ethane and propane generation (Cramer et al. 2001). Within the same temperature interval, Campbell (1978) detected the maximum generation rates of other low molecular weight condensable hydro-

carbons, mainly light aromatics, from subbituminous coal. This indicates that the modelled reaction II is related to the release of methyl groups by breaking of C–C bonds. These bond breaking reactions within the network structure of coal begin at temperatures of about 350 to 400 °C during gradual heating (Poutsma, 1990). This type of reaction is the most important process of alkane generation from humic organic matter in the catagenesis stage (Tissot and Welte, 1984).

Interestingly, the apparent stable carbon isotope signature of the initial methane precursor of reaction II ($\delta^{13}C = -30$ ‰, Table 1) differs significantly from that of the bulk organic carbon of the coal ($\delta^{13}C = -24.6$ ‰). This finding suggests that methyl carbon is isotopically lighter (about 5 ‰) than the average of carbon within the coal. These light isotope signatures of methane precursors possibly reflect isotopic effects during biosynthesis of the organic molecules (Clayton, 1991). Stepwise chemical degradation experiments of biogeochemical molecules showed that each carbon site of a hydrocarbon molecule can be distinguished by an individual stable carbon isotope signature, with differences in $\delta^{13}C$ values in some cases exceeding 5 ‰ (Monson and Hayes, 1982; Rossmann et al., 1991; Huang et al., 1999).

Reaction complex III: The identical ΔEa values of reactions II and III (Table 1) point to a similar reaction mechanism. Consequently, it is suggested that decomposition by cleavage of C–C bonds is the rate determining step also responsible for methane generation in reaction III.

With an apparent $\delta^{13}C$ of −25 ‰ the methane precursor of reaction III is close to the $\delta^{13}C$ of the bulk coal (−24.6 ‰), but significantly heavier than the precursor of reaction II. The same isotope pattern of methane precursors in kerogen as described for reaction complexes II and III (Table 1) was modelled by Clayton (1991). It was suggested, that methane from the reaction at higher temperature (reaction III) originates from the gas prone part of the kerogen which was termed refractory kerogen (Clayton, 1991). The similarity of the isotope signature between bulk kerogen and this precursor was interpreted to result due to the origin of the methane's carbon from alkyl groups which cross link aromatic and naphthenic structures (Jüntgen, 1985). Galimov (1985) expected these methane precursor groups to be slightly isotopically lighter than the mean isotope ratio of the macromolecular network.

Another possible source for methane from reaction III is the conversion of C_{2+}-hydrocarbons which were previously generated at lower temperatures (Cypres, 1976). Coal is a three-dimensional cross-linked molecular network in which pore openings are considered to be less than 5 Å (van Krevelen, 1961). Larger molecules are believed to be retained within the network. When a certain temperature is reached secondary cracking reactions are initiated. As a result, methane as the end product of this secondary cracking is released from the coal. Horsfield et al. (1992) showed that the spectrum of activation energies for cracking oil to gas has its maximum potential at approximately 270–285 kJ/mol (pre-exponential factor of $1.1 \cdot 10^{16}$ s^{-1}). This is in good agreement with the mean activation energy of reaction III of 270 kJ/mol (Table 1), supporting the idea of secondary cracking reactions within the coal as an important source of methane from reaction III. In addition, the precursor isotope signature of reaction III is close to the bulk isotope ratio and this is also consistent with secondary cracking, because long chain hydrocarbons are known to be isotopically similar to bulk organic matter (Chung et al., 1988; Mycke et al., 1994; Rooney et al., 1995).

Reaction complex IV: Reaction complex IV significantly influences the instantaneous isotopic composition of methane although the generation potential contributes only 6.6% to the total potential. Above 560 °C the $\delta^{13}C$ of methane starts to decrease indicating an admixture of isotopically light methane (Fig. 6). In the reaction kinetic model this isotopically light methane is realized by a $\delta^{13}C$ of the precursor of −31.5 ‰ (Table 1). With a ΔE of 30 J/mol reaction complex IV is characterized by the lowest difference in activation energy suggesting a significantly different reaction mechanism from all the other reactions. Friedrich and Jüntgen (1973) observed the same reversal in the methane isotope trend during open system pyrolysis experiments (Fig. 1) and assumed that reactions between aromatic substances in the coal might be responsible for the release of this late methane. This is in agreement with observations of peak benzene generation during late stage coal conversion which was interpreted to be due to pyrolysis of the remaining char residue rather than original low temperature coal depolymerization (Campbell, 1978). In this context, the low ΔE value of reaction IV can be interpreted to be caused by low isotope fractionation during the release of carbon from ring structures.

The observation of a light isotope signature of the methane precursor of reaction IV can be related directly to the reaction mechanism suggested. Aromatisation reactions release carbon from the macromolecular network which, as emphasized earlier, is expected to have the bulk isotope signature. However, only a small number of carbon sites must be released to reach a very high degree of aromatisation. So at the end of the reaction most of the carbon sites in the molecular structure were not involved in the reaction although they initially belonged to the group of possible precursor sites. Since the reaction preferentially removes the light isotope species first, the small group of carbon molecules released by the reaction is in fact significantly lighter than the entire group of possible precursor sites.

5. Concluding remarks

A mathematical model is presented which describes product generation and stable isotope fractionation in complexes of distributed first-order reactions. While Gaussian distributions were applied, the model can be calculated also with other probability functions. The model can be used to interpret isotope trends of natural gas components generated during laboratory pyrolysis experiments. In this context it enables the inference of reaction mechanisms for the generation of hydrocarbons and other products during the thermal decomposition of kerogen. Four reaction complexes were needed to model the generation of methane from coal. The underlying process of all reactions is believed to be the thermally induced unimolecular decomposition of macromolecules with free radical processes as the dominating reaction mechanism. However, differences between the respective modelled reaction complexes in the activation energy distributions, in the kinetic isotope effect and in the initial isotope inventory of the precursor suggest that the four reaction complexes differ in bond strength and in the type of precursor molecules. Nevertheless, it should be kept in mind that the mathematical model presented here is still a simplification of the complex processes during thermal decomposition of coal.

Applying the isotope specific reaction kinetic modelling to other gas species generated from coal (like ethane, ethene, propane, propene, carbon dioxide and carbon monoxide) a more detailed mass and isotope balance of the decomposition reactions will be possible.

Appendix A. First-order reaction kinetics of a single reaction

A 1. Single reaction—generation kinetics

Considering a system with a single first-order reaction where the reverse reaction is insignificant, the rate of product generation $r(t)$ for an arbitrary non-isothermal time-temperature history can be given as function of the rate coefficient $k(T(t))$ [Eq. (1)] and of the remaining reactant $f(t)$ at time t:

$$r(t) = \frac{\mathrm{d}c}{\mathrm{d}t} = -\frac{\mathrm{d}f}{\mathrm{d}t} = k(T(t)) \cdot f(t) \tag{A1}$$

Here the amount of reaction product $c(t)$ at time t is the difference between the initial amount of reactant f_0 and the concentration of the remaining reactant:

$$c(t) = f_0 - f(t) \tag{A2}$$

Considering only systems with a constant heating rate m (K/sec), for example non-isothermal pyrolysis experiments, the reaction rate can be related to temperature:

$$r(t) = m \cdot r(T) \tag{A3}$$

Applying this and integrating Eq. (A1) the amount of residual reactant $f(T)$ at temperature $T(t)$ can be obtained:

$$f(T) = f_0 \cdot \exp\left(-\frac{1}{m} \cdot \int_0^T k(T)dT\right) \tag{A4}$$

To calculate this reaction the evaluation of the temperature integral $I(T)$ of the rate coefficient [Eq. (A4)] is necessary:

$$I(T) = \int_0^T k(T)dT \tag{A5}$$

While numerical methods like the Simpson algorithm can be used, different approximations have been provided (e.g. Suuberg, 1983; Braun and Burnham, 1987). A manageable approximation of $I(T)$ for large values of $E/(G \cdot T)$ as well as initial temperatures low enough and final temperatures high enough that insignificant reaction rates occur was developed based on the Arrhenius type temperature dependence (van Heek and Jüntgen, 1968):

$$I(T) = G \cdot T^2 \cdot \frac{k(T)}{E} \tag{A6}$$

A 2. Single reaction—isotope kinetics

Isotope ratios are usually expressed as ratio of the heavy isotope species H to the light isotope species L:

$$R = \frac{H}{L} \tag{A7}$$

The calculations presented are performed in terms of these isotope ratios whereas the figures display isotope ratios in the more common Δ-notation. Δ-values relate the isotope ratio to a fixed standard ratio (R_{std}):

$$\delta[‰] = \left(\frac{R}{R_{\mathrm{std}}} - 1\right) \cdot 1000 \tag{A8}$$

For calculations of stable carbon isotope ratios as performed in this study the standard value is represented by the PDB-standard (Craig, 1957).

By relating the initial amounts of isotopic reactant species (f_{H0} and f_{L0}) according to Eq. (A7) the initial isotope ratio of the reactant or, in other words, the initial isotope ratio of the product precursor R_{prec0} can be defined:

$$R_{\mathrm{prec0}} = \frac{f_{H0}}{f_{L0}} \tag{A9}$$

In accordance with Eq. (A4) the isotope ratio of the precursor $R_{prec}(T)$ at an arbitrary temperature is the ratio of the remaining amounts of both isotope species of the reactant ($f_H(T)$ and $f_L(T)$)

$$\frac{R_{prec}(T)}{R_{prec0}} = \exp\left(\frac{1}{m}\cdot(I_L(T) - I_H(T))\right) \tag{A10}$$

By combining isotope specific versions of Eqs. (A1)–(A4) in a similar manner two isotope ratios of the product of a reaction can be defined which are the isotope ratio of the cumulative product $R_{cum}(T)$ as well as the isotope ratio of the instantaneously generated product $R_{inst}(T)$ at a given temperature T:

$$\frac{R_{cum}(T)}{R_{prec0}} = \frac{1-\exp\left(-\frac{I_H(T)}{m}\right)}{1-\exp\left(-\frac{I_L(T)}{m}\right)} \tag{A11}$$

$$\frac{R_{prec}(T)}{R_{inst}(T)} = KIE(T) \tag{A12}$$

Appendix B. First-order reaction kinetics of a distributed reaction

B 1. Distributed reaction—generation kinetics

Assuming a continuous probability function $D(E)$ of the activation energy the total fraction of reactant remaining $f(T)$ at temperature T for the distributed reaction is given with:

$$f(T) = f_0 \cdot \int_0^\infty \exp\left(\frac{-I(T,E)}{m}\right)\cdot D(E)dE \tag{B1}$$

The amount of the generated product and the generation rate of the distributed reaction complex can be calculated by substituting this form into Eqs. (A1) and (A2).

The density function $D(E)$ applied in this study is a Gaussian distribution:

$$D(E) = \frac{1}{\sigma\cdot\sqrt{2\cdot\pi}}\cdot\exp\left[-\frac{1}{2}\cdot\left(\frac{E-E_0}{\sigma}\right)^2\right] \tag{B2}$$

Here the density function is defined with E_0 denoting the mean activation energy of the distribution. σ is the Gaussian distribution parameter (standard deviation).

B 2. Distributed reaction—isotope kinetics

For a distributed reaction the isotope ratios of the precursor $R_{prec}(T)$, of the cumulative product $R_{cum}(T)$, and of the instantaneous product $R_{inst}(T)$ can be expressed by substituting Eq. (B2) into Eqs. (A10), (A11) and (A12). Eliminating the constant difference in activation energy ΔE, as well as the isotope specific pre-exponential factors from the integral, and combining these numbers to the $KIE(T)$ results for $R_{inst}(T)$ in a similar equation as Eq. (A12) with the $KIE(T)$ involved:

$$\frac{R_{prec}(T)}{R_{prec0}} = \frac{\int_0^\infty \exp\left(-\frac{I_H(T,E)}{m}\right)\cdot D(E)dE}{\int_0^\infty \exp\left(-\frac{I_L(T,E)}{m}\right)\cdot D(E)dE} \tag{B3}$$

$$\frac{R_{cum}(T)}{R_{prec0}} = \frac{1-\int_0^\infty \exp\left(-\frac{I_H(T,E)}{m}\right)\cdot D(E)dE}{1-\int_0^\infty \exp\left(-\frac{I_L(T,E)}{m}\right)\cdot D(E)dE} \tag{B4}$$

$$\frac{R_{prec0}}{R_{inst}(T)} = KIE(T)\cdot\frac{\int_0^\infty \exp\left(-\frac{E}{G\cdot T}-\frac{I_L(T,E)}{m}\right)\cdot D(E)dE}{\int_0^\infty \exp\left(-\frac{E}{G\cdot T}-\frac{I_H(T,E)}{m}\right)\cdot D(E)dE} \tag{B5}$$

Appendix C. First-order reaction kinetics of combined reaction complexes

Considering a combined reaction complex in which i independent reactant pools contribute to the overall reaction, the fraction of the initial product precursor is the sum of the precursors of the individual reaction systems:

$$f_0 = \sum_{n=1}^{i} f_{i0} \tag{C1}$$

According to Eq. (A9) the overall instantaneous isotope inventory R_{prec0} contributing to the product can be defined as:

$$R_{prec0} = \frac{\sum_{n=1}^{i} f_{iH0}}{\sum_{n=1}^{i} f_{iL0}} \tag{C2}$$

The overall isotope ratios of the precursor, the instantaneous product, as well as the cumulative product at a certain temperature can then be expressed in a similar way considering Eqs. (A10), (A11), and (A12).

Appendix D. Table of abbreviations

T	temperature
t	time
k	rate coefficient
A	pre-exponential factor
E	activation energy
G	gas constant [8.3145 J/K/mol]
$_L$	index light isotope species
$_H$	index heavy isotope species
r	rate of product generation
c	amount of cumulative reaction product
f_0	initial amount of reactant
f	amount of reactant
m	heating rate
$I(T)$	temperature integral
R	isotope ratio
$_{prec}$	index for the precursor of the reaction
$_{inst}$	index for the instantaneous product of the reaction
$_{cum}$	index for the cumulative product of the reaction
δ	standard isotope ratio [‰]
D	distribution function
σ	Gaussian distribution parameter

References

Anthony, D.B., Howard, J.B., 1976. Coal devolatilization and hydrogasification. AIChE Journal 22 (4), 625–656.

Berner, U., Faber, E., 1996. Empirical carbon isotope/maturity relationships for gases from algal kerogens and terrigenous organic matter, based on dry, open-system pyrolysis. Organic Geochemistry 24 (10-11), 947–955.

Berner, U., Faber, E., Scheeder, G., Panten, D., 1995. Primary cracking of algal and landplant kerogens: kinetic models of isotope variations in methane, ethane and propane. Chemical Geology 126, 233–245.

Bigeleisen, J., 1949. The relative reaction velocities of isotopic molecules. Journal of Chemical Physics 17 (8), 675–677.

Braun, R.L., Burnham, A.K., 1987. Analysis of chemical reaction kinetics using a distribution of activation energies and simpler models. Energy & Fuels 1, 153–161.

Burnham, A.K., Braun, R.L., 1999. Global kinetic analysis of complex materials. Energy & Fuels 13 (1), 1–22.

Burnham, A.K., Braun, R.L., Gregg, H.R., 1987. Comparison of methods for measuring kerogen pyrolysis rates and fitting kinetic parameters. Energy & Fuels 1, 452–458.

Campbell, J.H., 1978. Pyrolysis of subbituminous coal in relation to in-situ coal gasification. Fuel 57, 217–224.

Chung, H.M., Gormly, J.R., Squires, R.M., 1988. Origin of gaseous hydrocarbons in subsurface environments: theoretical considerations on carbon isotope distribution. Chemical Geology 71, 97–103.

Clayton, C., 1991. Carbon isotope fractionation during natural gas generation from kerogen. Marine and Petroleum Geology 8, 232–240.

Craig, H., 1957. Isotopic standards for carbon and oxygen and correction factors for mass-spectrometric analysis of carbon dioxide. Geochimica et Cosmochimca Acta 12, 133–149.

Cramer, B., Faber, E., Gerling, P., Krooss, B.M., 2001. Reaction kinetics of stable carbon isotopes in natural gas- insights from dry, open-system pyrolysis experiments. Energy & Fuels 15, 517–532.

Cramer, B., Krooss, B.M., Littke, R., 1998. Modelling isotope fractionation during primary cracking of natural gas—a reaction kinetic approach. Chemical Geology 149, 235–250.

Cypres, R., 1976. Reaktionsmechanismen bei der Pyrolyse und Aromatisierung von Teerbestandteilen. In: Proceedings of 4. Gemeinschaftstagung ÖGEW/DGMK, pp. 435-453, Salzburg.

del Rio, J.C., Gonzalez-Vila, F.J., Martin, F., Verdejo, T., 1994. Characterization of humic acids from low-rank coals by ^{13}C-NMR and pyrolysis-methylation. Formation of benzenecarboxylic acids moieties during the coalification process. Organic Geochemistry 22 (6), 885–891.

Faber, E., 1987. Zur Isotopengeochemie gasförmiger Kohlenwasserstoffe. Erdöl Erdgas Kohle Zeitschrift 103 (5), 210–218.

Friedrich, H.-U., Jüntgen, H., 1973. Aussagen zum $^{13}C/^{12}$-Verhältnis des bei der Inkohlung gebildeten Methans aufgrund von Pyrolyseversuchen. Erdöl und Kohle–Erdgas–Petrochemie vereinigt mit Brennstoff-Chemie 26 (11), 636–639.

Galimov, E.M., 1974. Characteristics of the kinetic isotope effect in the degradation of organic matter. Zhurnal Fizicheskoj Khimii 48 (6), 811–814.

Galimov, E.M., 1985. The Biological Fractionation of Isotopes. Academic Press, London.

Galimov, E.M., 1988. Sources and mechanisms of formation of gaseous hydrocarbons in sedimentary rocks. Chemical Geology 71, 77–95.

Gaveau, B., Letolle, R., Monthioux, M., 1987. Evaluation of kinetic parameters from ^{13}C isotopic effect during coal pyrolysis. Fuel 66, 228–231.

Hanbaba, P., Jüntgen, H., Peters, H., 1968. Nicht-isotherme Reaktionskinetik der Kohlenpyrolyse, Teil II: Erweiterung der Theorie der Gasabspaltung und experimentelle Bestätigung an Steinkohlen. Brennstoff-Chemie 49 (12), 368–376.

Horsfield, B., Schenk, H.J., Mills, N., Welte, D.H., 1992. An investigation of the in-reservoir conversion of oil to gas: compositional and kinetic findings from closed-system programmed-temperature pyrolysis. Organic Geochemistry 19 (1-3), 191–204.

Huang, D.-S., Wu, S.-H., Huang, C.-Y., Lin, C.-Y., 1999. An exploration of intramolecular isotopic distributions of commercial acetone and isopropanol. Organic Geochemistry 30, 667–674.

Jüntgen, H., van Heek, K.H., 1970. Reaktionsabläufe unter nicht-isothermen Bedingungen. Fortschritte der Chemischen Forschung 13 (3-4), 601–699.

Jüntgen, H., 1964. Reaktionskinetische Überlegungen zur Deutung von Pyrolyse-Reaktionen. Erdöl und Kohle, Erdgas, Petrochemie 17 (3), 180–186.

Jüntgen, H., 1985. Zum Mechanismus von Pyrolyse und Hydropyrolyse. Erdöl und Kohle–Erdgas–Petrochemie vereinigt mit Brennstoff-Chemie 38 (10), 448–455.

Kröger, C., Brücker, R., 1961. Über die physikalischen und chemischen Eigenschaften der Steinkohlegefügebestandteile XV.—Hochvakuumpyrolyse und Kohlekonstitution. Brennstoff-Chemie 42 (10), 305–311.

Lakshmanan, C.C., Bennett, M.L., White, N., 1991. Implications of multiplicity in kinetic parameters to petroleum exploration: distributed activation energy models. Energy & Fuels 5, 110–117.

Lorant, F., Prinzhofer, A., Behar, F., Huc, A.-Y., 1998. Carbon isotopic and molecular constrains on the formation and the expulsion of thermogenic hydrocarbon gases. Chemical Geology 147, 249–264.

Monson, K.D., Hayes, J.M., 1982. Biosynthetic control of the abundance of carbon 13 at specific positions within fatty acids in *Saccharomyces cerevisiae*—isotopic fractionation in lipid synthesis as evidence for peroxisomal regulation. The Journal of Biological Chemistry 257 (10), 5568–5575.

Mycke, B., Hall, K., Leplat, P., 1994. Carbon isotopic composition of individual hydrocarbons and associated gases evolved from micro-scale sealed vessel (MSSV) pyrolysis of high molecular weight organic material. Organic Geochemistry 21 (6-7), 787–800.

Payne, D.F., Ortoleva, P.J., 2001. A model for lignin alteration —part I: a kinetic reaction-network model. Organic Geochemistry 32, 1073–1085.

Poutsma, M.L., 1990. Free-radical thermolysis and hydrogenolysis of model hydrocarbons relevant to processing of coal. Energy & Fuels 4 (2), 113–131.

Prinzhofer, A., Pernaton, E., 1997. Isotopically light methane in natural gas: bacterial imprint or diffusive fractionation. Chemical Geology 142, 193–200.

Rohrback, B.G., Peters, K.E., Kaplan, I.R., 1984. Geochemistry of artificially heated humic and sapropelic sediments—II: oil and gas generation. American Association of Petroleum Geologists Bulletin 68 (8), 961–970.

Rooney, M.A., Claypool, G.E., Chung, H.M., 1995. Modeling thermogenic gas generation using carbon isotope ratios of natural gas hydrocarbons. Chemical Geology 126, 219–232.

Rossmann, A., Butzenlechner, M., Schmidt, H.-L., 1991. Evidence for a nonstatistical carbon isotope distribution in natural glucose. Plant Physiology 96, 609–614.

Schenk, H.J., Horsfiel, B., Krooss, B., Schaefer, R.G., Schwochau, K., 1997. Kinetics of petroleum formation and cracking. In: Welte, D.H., Horsfield, B., Baker, D.R. (Eds.), Petroleum and Basin Evolution. Springer, Berlin, Heidelberg, New York, pp. 231–269.

Schoell, M., 1980. The hydrogen and carbon isotopic composition of methane from natural gases of various origins. Geochimica et Cosmochimica Acta 44, 649–661.

Smith, J.W., Rigby, D., Gould, K.W., Hart, G., Hargraves, A.J., 1985. An isotopic study of hydrocarbon generation processes. Organic Geochemistry 8 (5), 341–347.

Spindel, W., Stern, M.J., Monse, E.U., 1970. Further studies on temperature dependences of isotope effects. Journal of Chemical Physics 52 (4), 2022–2035.

Stahl, W.J., Carey, B.D.J., 1975. Source-rock identification by isotope analyses of natural gases from fields in the Val Verde and Delaware basins, West Texas. Chemical Geology 16, 257–267.

Stern, M.J., Spindel, W., Monse, E.U., 1968. Temperature dependence of isotope effects. Journal of Chemical Physics 48 (7), 2908–2919.

Sundararaman, P., Merz, P.H., Mann, R.G., 1992. Determination of kerogen activation energy distribution. Energy & Fuels 6, 793–803.

Suuberg, E.M., 1983. Approximate solution technique for nonisothermal, Gaussian distributed activation energy models. Combustion and Flame 50, 243–245.

Tang, Y., Perry, J.K., Jenden, P.D., Schoell, M., 2000. Mathematical modeling of stable carbon isotope ratios in natural gas. Geochimica et Cosmochimica Acta 64 (15), 2673–2687.

Tissot, B., 1969. Premieres donnees sur les mecanismes et la cinetique de la formation du petrole dans les sediments. Simulation d'un schema reactionnel sur ordinateur. Revue de l'Institute Francais du Petrole 24, 470–501.

Tissot, B., Welte, D.H., 1984. Petroleum Formation and Occurrence. Springer, Berlin, Heidelberg, New York.

van Heek, K.H., Jüntgen, H., 1968. Bestimmung der reaktionskinetischen Parameter aus nicht-isothermen Messungen. Berichte der Bunsengesellschaft Physik und Chemie 72, 1223–1231.

van Heek, K.H., Kassler, P., Wanzl, W., 1986. Übertragung von Laborergebnissen zur Pyrolysekinetik von Kohlen auf in situ-Reaktionen. Erdöl Erdgas Kohle 102 (4), 200–205.

van Krevelen, D.W., 1961. Coal Typology—Chemistry–Physics–Constitution. Elsevier, Amsterdam.

van Krevelen, D.W., van Heerden, C., Huntjes, F.J., 1951. Physiochemical aspects of the pyrolysis of coal and related organic compounds. Fuel 30, 253–259.

Whiticar, M.J., Faber, E., Schoell, M., 1986. Biogenic methane formation in marine freshwater environments: CO_2 reduction vs. acetate fermentation—isotope evidence. Geochimica et Cosmochimica Acta 50, 693–709.